Multi-strap In-port ICRF Antenna Modeling and Development in Support of ITER and EU-DEMO

Volodymyr Bobkov[1, a)], Roberto Bilato[1], François Calarco[2], Helmut Faugel[1], Oleksii Girka[1], Walid Helou[2], Philippe Lamalle[2], Vincent Maquet[3], Daniele Milanesio[4], Roman Ochoukov[1], Vincent Polli[5], Wouter Tierens[1], Maria Usoltseva[1], Wei Zhang[1,6]

[1]*Max-Planck-Institut für Plasmaphysik, Garching, Germany*
[2]*ITER Organization, Route de Vinon-sur-Verdon, CS 90 046, 13067 St. Paul Lez Durance Cedex, France*
[3]*Laboratory for Plasma Physics, ERM-KMS, 1000 Brussels, Belgium, TEC Partner*
[4]*Politecnico di Torino, Corso Duca degli Abruzzi, 24, 10129 Torino TO, Italia*
[5]*Capgemini Engineering, Parc du Golf – Bat.17, 350 Av JRG Gautier de la Lauziere, CS40514, 13593 Aix en Provence Cedex 3, France*
[6]*Institute of Plasma Physics, Chinese Academy of Sciences, Hefei 230031, China*

[a)] Corresponding author: bobkov@ipp.mpg.de

Abstract. Full-size 3D model of ITER ICRF antenna with 1D plasma electron density (n_e) and 3D n_e (from EMC3-Eirene) was simulated using the RAPLICASOL (COMSOL-based) code. Impedance matrices and coupled power agree well with TOPICA with 1D n_e. Cases with 3D n_e show port-to-port differences compared to 1D n_e, as well as a lower (about 10%) coupled power. Efficient minimization of ITER antenna near-fields (to reduce RF sheaths by optimizing feeding) calculated by TOPICA and RAPLICASOL is possible with [0;π;π;0] (about balanced strap powers) and is even lower with [0;π;0;π] toroidal phasing (with dominant power from central straps). Lowest near-fields are with [0;π] poloidal phasing, but [0;-π/2] will be used in a load resilience setup with 3dB splitters. Under EUROfusion prospective research and development, in-port ICRF antenna concept for EU-DEMO with 8 quadruplets (4x toroidal by 2x poloidal) is considered to deliver 16.7 MW (3 antennas yielding 50 MW). Areas around the equatorial port and cut-ins in breeding blankets are used, with emphasis on [0;π;π;0] optimization. High-resolution RAPLICASOL calculations with full n_e profile (without imposing a minimum n_e value) shed light on field distribution with propagative slow wave in detailed antenna geometry.

1. INTRODUCTION

During the finalization of ITER ICRF (Ion Cyclotron Range of Frequencies) antenna design in the period between 2020 and 2022, the modern simulation tools TOPICA [1] and RAPLICASOL [2] (COMSOL-based [3]) were applied to predict key RF properties for the future antenna operation in ITER. In this paper, an overview is given on the activities in IPP Garching on this modelling of the ITER ICRF antenna, as well as on development of a proposed in-port antenna for EU-DEMO [4]. The latter builds on a similar approach as the ITER antenna, with modifications imposed by additional geometrical boundary conditions. The focus of the work is on two main aspects: 1) maximization of coupled power P_{coup}; and 2) minimization of the local linear parallel electric field $E_{||}$ drive of RF sheaths and Plasma Wall Interactions (PWI) at Plasma Facing Components (PFCs) [5] at the best compromise with (1). As in the previous assessments [6], the local $E_{||}$ drive is calculated by an EM code in a vacuum layer just in front of the PFCs. The use of the local $E_{||}$ values for minimization of PWIs implies the condition of the evanescent Slow Wave (SW) at the PFCs [6]. However, as is discussed at the end of paper, this condition is not necessarily valid for all the density profiles predicted for the future devices and SW propagation is possible.

2. RESULTS AND DISCUSION

2.1 Calculations with RAPLICASOL and comparison with TOPICA

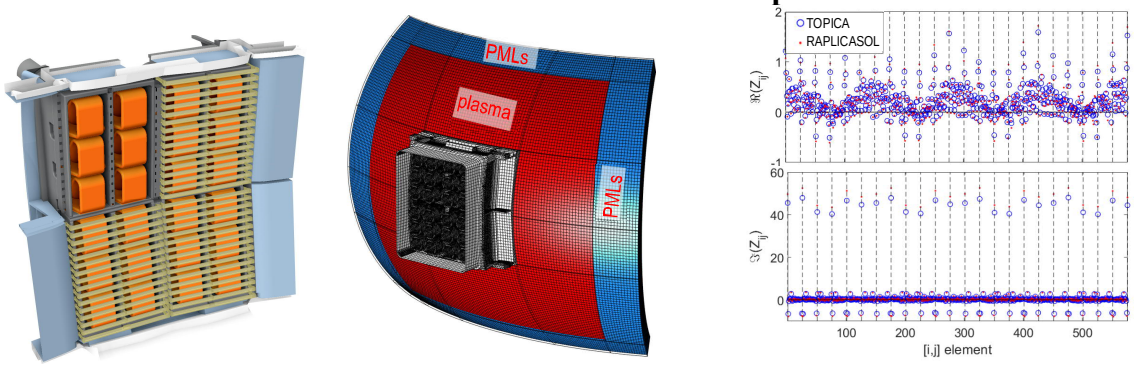

(a) (b)

FIGURE 1. *a) 24-port ITER antenna model (left) and RAPLICASOL grid including plasma and PML regions (right). b) Comparison of real (upper) and imaginary (lower) parts of impedance for 24x24 matrix elements for 55 MHz, "large gap" case. Blue circles: TOPICA, Red dots: RAPLICASOL.*

The RAPLICASOL and TOPICA codes have agreed well in the previous studies [7]. This section briefly summarizes some of the results of the ITER ICRH antenna simulations with the codes and their comparisons. A detailed paper on the results will be published independently [8]. Figure 1(a) shows the full-size 24-port model of the ITER antenna used in TOPICA and RAPLICASOL together with the RAPLICASOL grid and the calculation domain setup. The setup includes the cold plasma region surrounded by Perfectly Matched Layers (PMLs) where the power is absorbed, in the same manner as at the outward radiation boundary of the FELICE plasma module of TOPICA. Similarly to TOPICA, the minimum density is restricted in the plasma regions of RAPLICASOL above the lower-hybrid density, in an attempt to avoid numerical issues close to the lower-hybrid resonance. Impedance matrices are compared between TOPICA and RAPLICASOL in Fig. 1(b) for the case of the 1D radial plasma electron density (n_e) distribution with the 55 MHz, "large gap" (low n_e) case. The values agree well between the two codes, considering their different formulations and consequently, deviations in boundary conditions. The good agreement is further confirmed by the comparison of P_{coup} for various toroidal and for two poloidal ([0;-π/2], [0;π]) phasings imposed at the antenna ports, shown in Fig. 2(a). In all the toroidal phasings, apart from the monopole, the agreement is within few percent. Values of P_{coup} are generally higher with poloidal [0;π] (corresponds to the monopole poloidal phasing for the currents at the antenna straps), but [0;-π/2] will be imposed in ITER by the experimental setup of each independent antenna using the 3dB splitters for load resilience.

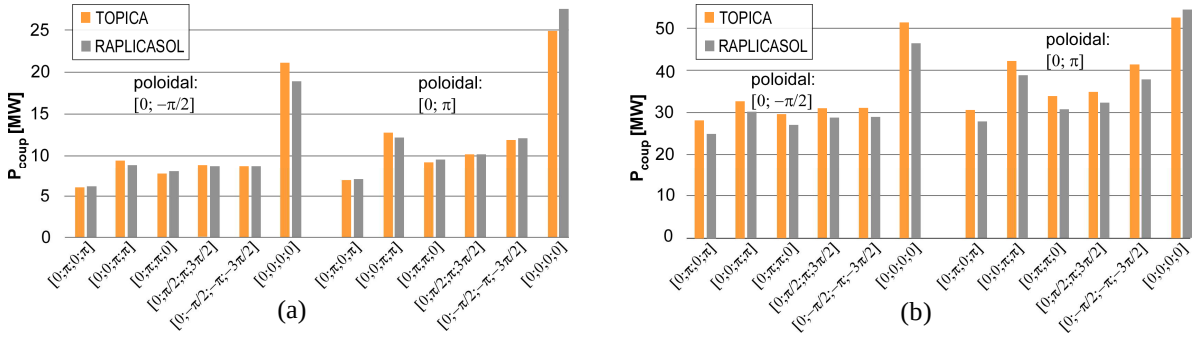

FIGURE 2. *Comparison between TOPICA and RAPLICASOL. (a) "Large gap" 55MHz with 1D n_e. (b) Midplane gas injection, TOPICA with poloidally and toroidally averaged 1D n_e, RAPLICASOL with full 3D n_e.*

Using RAPLICASOL, similarly to [9] the cases are extended to the 3D n_e distribution which is deduced from the EMC3-Eirene code [10] for the case with strong midplane gas injection close to the antennas and improved P_{coup}. This case shown in Fig. 2(b) represents one of the most inhomogeneous n_e distributions for the port 13 ITER ICRH antenna. For TOPICA, poloidal and toroidal averaging are applied to produce radial 1D n_e, whereas RAPLICASOL operates with full 3D n_e. The 3D RAPLICASOL cases have calculated P_{coup} by about 10% lower than the spatially averaged 1D cases of TOPICA.

The appearance of the n_e inhomogeneity leads to individual changes of the effective loading resistances of the 24 feeders of the antenna model. Comparing relative changes of the resistances between the RAPLICASOL calculations with the spatially-averaged 1D n_e and with the full 3D n_e, the largest decrease of up to 40 % is experienced by the upper half of the feeders, whereas the resistances of the feeders in the lower half mostly increase by up to 15%. With small variations, this is the case both for the port 13 and for the port 15 ITER ICRH antennas.

2.2 Near-field analysis

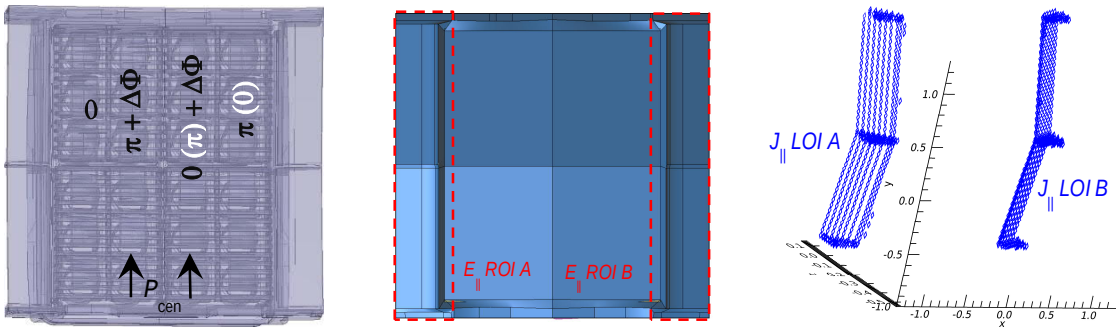

(a) (b) (c)

FIGURE 3. *a) Scheme of feeding law variation; b) Regions Of Interest (ROI) for $E_{||}$; c) Locations Of Interest (LOI) for $J_{||}$ with positions of the LOI mesh elements shown by diamond symbols.*

Based on the TOPICA and RAPLICASOL calculations, $E_{||}$ and to some extent the parallel component of the RF current $J_{||}$ flowing at PFCs are analyzed as a function of feeding law variations close to the toroidal phasings of [0;π;π;0] and [0;π;0;π]. Relative differences of $E_{||}$ and $J_{||}$ guide the minimization of the PWI at the PFCs. As it is shown in Fig. 3(a), the scan of the feeding law includes a scan of the power balance, i.e. the power coupled by the both central columns of straps P_{cen} w.r.t. the total coupled power P_{coup}, and a scan of phase with deviation from the nominal dipole phasing ΔΦ=±45°. The forward voltages are fixed equal for the two central strap columns and, independently, equal for the outer strap columns. The phase is defined between the forward voltages. Values of $E_{||}$ and $J_{||}$ are normalized to the maximum voltage in the Transmission Lines (TLs) of 45 kV peak. Values of $E_{||}$ are averaged over the Regions Of Interest (ROI) just in front of the lateral PFCs (see Fig. 3(b)) and values of $J_{||}$ are averaged over the grid on the lateral PFCs, Locations of Interest (LOI) (see Fig. 3(c) with the LOI mesh element positions shown by diamond symbols). Behavior of the maximum $E_{||}$ values was also analyzed: it has similar tendencies as that of the averaged values (see below) with some deviations and will be reported elsewhere.

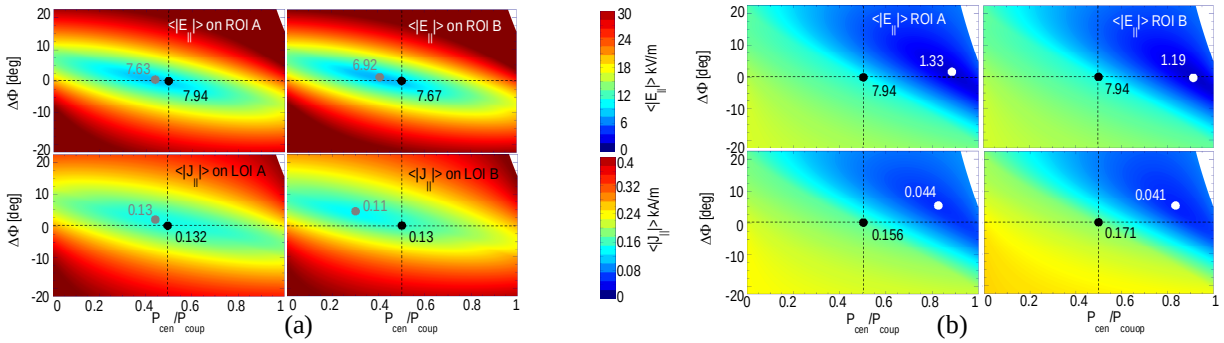

FIGURE 4. *<$E_{||}$> on ROIs (upper row) and <$J_{||}$> on LOIs (lower row) as functions of P_{cen}/P_{coup} and ΔΦ with [0;-π/2] poloidal, normalized to the maximum voltage in TLs of 45 kV peak, TOPICA, 55 MHz, "large gap": a) [0;π;π;0]; b) [0;π;0;π].*

Figure 4 presents the analysis and the minimum values of $E_{||}$ and $J_{||}$ derived from TOPICA as a function of the feeding law variations for [0;π;π;0] and [0;π;0;π], both with [0;-π/2] poloidal phasing, for the case of 55 MHz, "large gap". Spatially averaged <$E_{||}$> in front of the PFCs is consistent with, or in other words driven by <$J_{||}$> on the PFCs. Minimization of both is possible by adjusting the feeding away from nominal ΔΦ=0°, P_{cen}/P_{coup}=0.5, with lowest values achievable at [0;π;0;π], but with strongly reduced P_{coup}, mostly launched by the center straps. On the other hand, [0;π;π;0] offers a compromise close to the balanced power antenna operation.

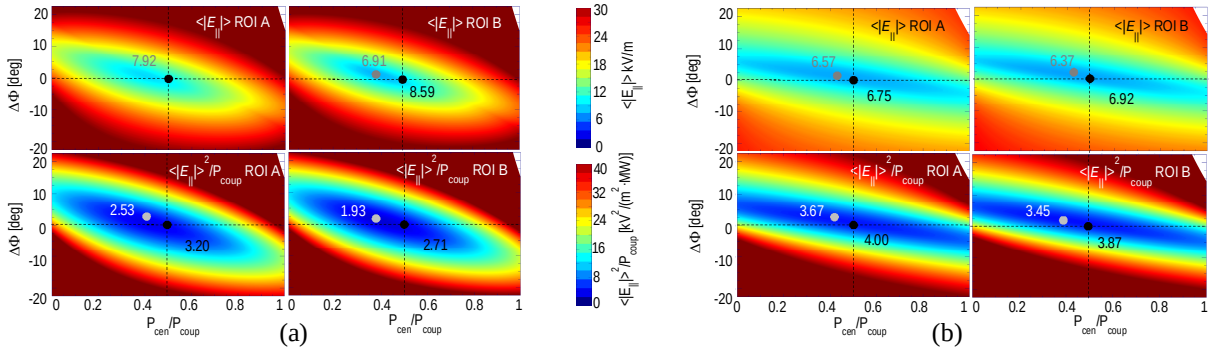

FIGURE 5. *<$E_{||}$> on ROIs (upper row) and <$E_{||}$>^{2}/P_{coup} (lower row) as functions of P_{cen}/P_{coup} and $\Delta\Phi$ with [0;π;π;0] toroidal and [0;-π/2] poloidal, TOPICA data: a) high coupling (midplane injection); b) low coupling (divertor injection).*

It is often expected that the near-fields are reduced when coupling is improved. Figure 5, derived with TOPICA data for 55 MHz, demonstrates that this is not always the case, and it can be a matter of normalization. When the fields are normalized to 45 kV peak in TLs and the main mechanism of $E_{||}$ excitation is electromagnetic (in our case driven by $J_{||}$), <$E_{||}$> is higher for the high coupling scenario with the midplane gas injection ($P_{coup} > P_{coup\ \text{"large gap"}}$) in Fig. 5(a), compared to the low coupling scenario with the divertor gas ($P_{coup} < P_{coup\ \text{"large gap"}}$) in Fig. 5(b). At the same time, a quadratic normalized quantity <$E_{||}$>^{2}/P_{coup} (lower row of Fig. 5) is lower for the high coupling, i.e. at a given power <$E_{||}$> is lower. However, generally there can be cases characterized by higher <$E_{||}$> at higher coupling even at the same power. This will be reported elsewhere. Figure 5 shows another prominent feature – a spread of the minima of <$E_{||}$> and <$E_{||}$>^{2}/P_{coup} over a larger range of P_{cen}/P_{coup} at lower coupling. This can be attributed to the stronger relative role of the cross-coupling between the neighboring columns of straps at low coupling.

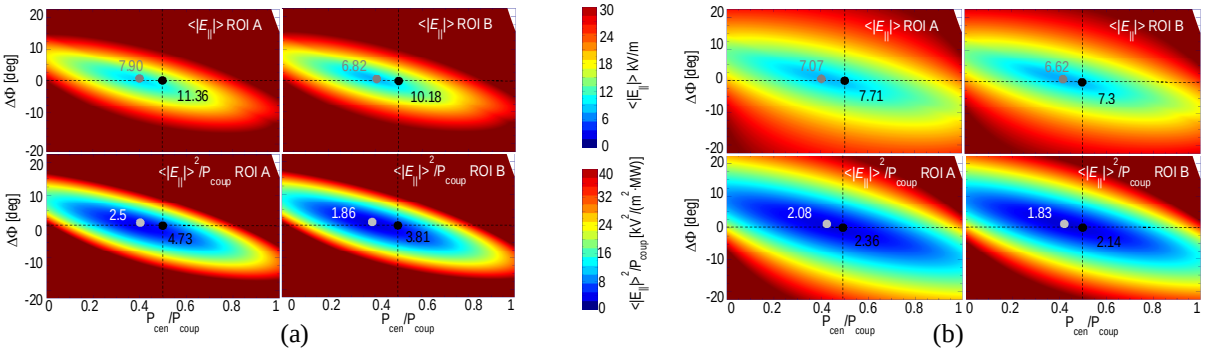

FIGURE 6. *<$E_{||}$> on ROIs (upper row) and <$E_{||}$>^{2}/P_{coup} (lower row) as functions of P_{cen}/P_{coup} and $\Delta\Phi$ with [0;π;π;0] toroidal and [0;-π/2] poloidal, RAPLICASOL data: a) 1D n_e; b) 3D n_e.*

Figure 6 shows the difference between the <$E_{||}$> calculations with 1D n_e and that with 3D n_e for the most inhomogeneous n_e case with the midplane gas injection close to the ICRH antenna in port 13 operated at 55 MHz. The difference in optimization is not significant close to the minima of <$E_{||}$> and <$E_{||}$>^{2}/P_{coup} and is more noticeable away from the minima where the quantities are lower in the case with 3D n_e.

Figure 5(a) and Fig. 6(a) point out the differences in <$E_{||}$> and <$E_{||}$>^{2}/P_{coup} between TOPICA and RAPLICASOL. Again, the values agree excellently at the minima, but less so further away.

The effect of the poloidal phasing on <$E_{||}$>^{2}/P_{coup} is shown in Fig. 7 for the case of 55 MHz, "large gap". The quantity is significantly lower with the poloidal phasing of [0;π], and both the reduction of <$E_{||}$> and the increase of P_{coup} (see Fig. 2(a) for <$E_{||}$> in this case) contribute to this change. However, as mentioned above, the poloidal phasing is restricted to [0;-π/2], because the antennas are required to operate independently from each other with the 3dB splitter scheme for the load resilience. Interesting to note is that the feeding parameters for the minimum of <$E_{||}$>^{2}/P_{coup} at [0;π] are quite different to those at [0;-π/2] (same applies to <$E_{||}$>).

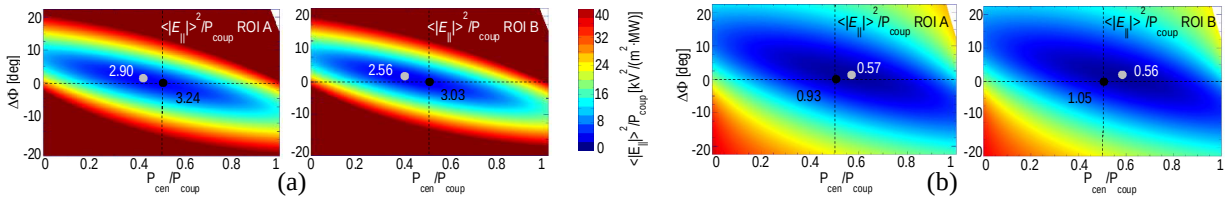

FIGURE 7. *$\langle E_{\parallel}\rangle^2/P_{coup}$ with [0;π;π;0], from TOPICA data: a) [0;-π/2] poloidal; b) and [0;π] poloidal.*

2.3 Development of in-port antenna concept for EU-DEMO and coping with low n_e

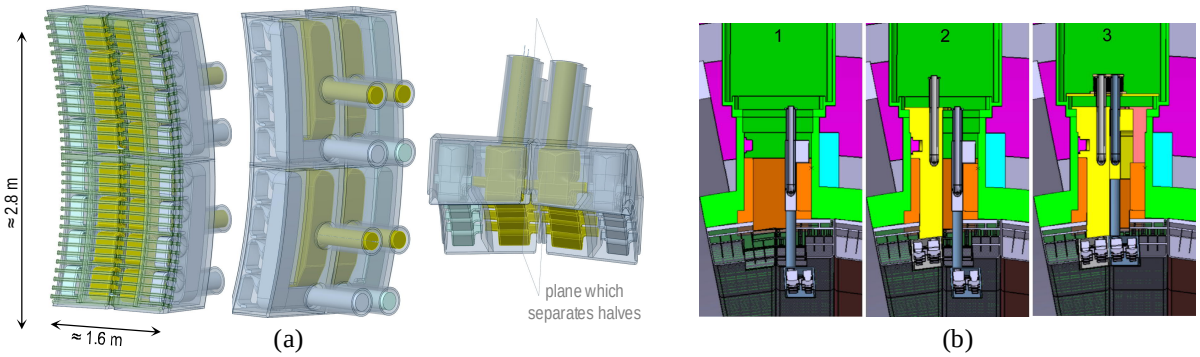

FIGURE 8. *a) Full curved model of the TAH antenna with isometric views from the plasma side, from the back side and from the top; b) top view of simplified installation steps of the TAH antenna into the vessel via the equatorial port.*

Currently, within the EUROfusion consortium, the mainstream choice of heating and current drive methods for EU-DEMO is based on the sole use of ECRH power [11]. ICRF heating is a part of the prospective research and development program, considered as an option mainly aimed at ion heating and assistance to enter into high confinement regimes [12]. For ICRF, our focus is on the in-port mounted ITER-type antennas which are to be installed into the torus vessel independently of the breeding blanket modules. The travelling wave ICRF antenna which requires a deep integration with the blanket modules, is currently considered as a backup option for an eventual ICRF system at EU-DEMO and is described elsewhere [13].

The requirement of the in-port installation and limited dimensions of equatorial ports limits the area of possible ICRF antennas. The most realistic compromise found so far to achieve a larger area for radiating ICRF antenna elements is by using some of the volume of the breeding area around the equatorial port, although this imposes additional constraints on the blanket module structure. The ICRF antenna is split into Toroidally Arranged Halves (TAH) shown in Fig. 8(a) which are installed one after the other as it is shown in Fig. 8(b) in three simplified steps. In order to couple 50 MW from 3 antennas, the power density of about 3.9 MW/m^2 would be required for the considered geometrical boundary conditions [14]. The ITER "large gap" n_e profile is taken as a reference. It represents a predicted EU-DEMO n_e profile, revealed to be almost identical to the ITER one in flux coordinates, and shifted closer to the antenna by local gas injection techniques. The calculations show [11,15] that it is possible to couple the requested power by using straps based on 4 segments (quadruplets) as opposed to the triplets at ITER and by reducing $k_{\parallel}$ to about 4 m^{-1}. The antenna presented in Fig. 8(a) incorporates this by using 8 quadruplets. The antenna is optimized for [0;π;π;0] toroidal phasing by making the central straps large to reduce the dominant $k_{\parallel}$, and by the inclined septa to help balancing out the image current contributions and $E_{\parallel}$ on the antenna lateral sides in order to minimize PWI at the power fraction launched by the central strap close to 0.5.

Due to low expected n_e at the PFCs for some ITER cases and for DEMO, SW is propagative close to PFCs. Figure 9 shows an example of the propagative SW affecting the near-field. A model was used with a small section of the ITER-type antenna with 2 toroidally arranged [0;π]-phased strap segments without a Faraday screen, but with PFCs (see Fig. 9(a)), with a perfect electric conductor boundary condition on the symmetry plane, effectively representing 4 toroidal strap segments with [0;π;0;π] phasing. High-resolution RAPLICASOL calculations were then performed following the approach in [16]. The SW propagation on a toroidal-radial plane of this detailed geometry can be seen in Fig. 9(b): the straps and the antenna frame launch the Resonance Cones (RCs) propagating towards the low-hybrid resonance where the power is absorbed by collisions or by PMLs surrounding the calculation frame. The near-field (toroidal component E_z) at the PFCs is dependent on the properties of the RCs.

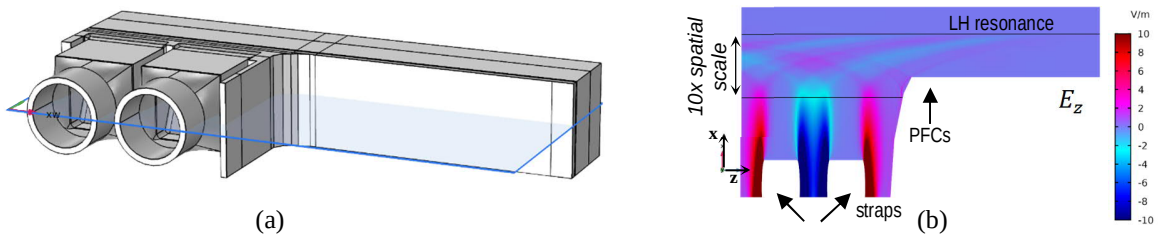

FIGURE 9. *a) Screenless ITER-type antenna section for high-resolution RAPLICASOL simulations with a plane of interest; b) slow wave propagation at low n_e in front of the antenna as seen from toroidal electric field E_z.*

3. CONCLUSIONS

The full-size ITER antenna models were used in simulations by the well-agreeing TOPICA and RAPLICASOL codes, with the latter extending the calculations to the full 3D density distribution that yields about 10% lower coupled power in the midplane gas puff cases with the most inhomogeneous density.

The parallel RF electric field at the PFCs, mainly driven electromagnetically by the parallel component of RF current can be reduced well by optimizing feeding law to minimize PWI. The minimization is particularly efficient at the [0;π;0;π] toroidal phasing with the power mostly launched by the central two columns of the straps thus reducing the available total power, and at [0;π] poloidal phasing which cannot be used under the ITER requirements of independent operation of antennas and load resilience. The configuration of [0;π;π;0] toroidal and [0;-π/2] poloidal offers a fair compromise to deliver high ICRF power and minimize PWI.

An optional in-port ICRF antenna is being developed for EUROfusion EU-DEMO based on ITER antenna concept and further optimizations for heating in [0;π;π;0] phasing with efficiently minimized PWI. High-resolution RAPLICASOL calculations demonstrate that in detailed geometry, for the low density at the PFCs, the full-wave near-fields can be affected by the propagating SW in a complicated pattern. Future work is needed to assess this.

ACKNOWLEDGMENTS

The work presented in sections 2.1 and 2.2 has been conducted under IO contracts IO/20/CT/4300002150, IO/20/CT/4300002118 and IO/20/CT/4300002178. The views and opinions expressed herein do not necessarily reflect those of the ITER Organization.

The work presented in section 2.3 has been carried out within the framework of the EUROfusion Consortium, funded by the European Union via the Euratom Research and Training Programme (Grant Agreement No 101052200 — EUROfusion). Views and opinions expressed are however those of the author(s) only and do not necessarily reflect those of the European Union or the European Commission. Neither the European Union nor the European Commission can be held responsible for them.

REFERENCES

1. D. Milanesio et al., Nuclear Fusion **49** (11) (2009) 115019, https://doi.org/10.1088/0029-5515/49/11/115019
2. J. Jacquot et al., AIP Conf. Proc. **1689** (2015) 050008, https://doi.org/10.1063/1.4936496
3. COMSOL, https://www.comsol.com
4. M. Usoltceva et al., Fus. Eng. Des. **165** (2021) 112269, https://doi.org/10.1016/j.fusengdes.2021.112269
5. V. Bobkov et al., Nuclear Materials and Energy **18** (2018) 131-140, https://doi.org/10.1016/j.nme.2018.11.017
6. V. Bobkov et al., Plasma Phys. Control. Fusion **59** (2017) 014022, https://doi.org/10.1088/0741-3335/59/1/014022
7. W. Tierens et al., Nucl. Fusion **59** (2019) 046001, https://doi.org/10.1088/1741-4326/aaf455
8. W. Tierens et al., "ICRF code benchmarks for the ITER antenna; first non-axisymmetric cases", to be submitted
9. W. Tierens et al., EPJ Web of Conferences **157** (2017) 03053, https://doi.org/10.1051/epjconf/201715703053
10. W. Zhang et al., "Parametric study of midplane gas puffing to maximize ICRF power coupling in ITER", submitted to Nuclear Fusion
11. M. Q. Tran et al., Fus. Eng. Des. **180** 113159, https://doi.org/10.1016/j.fusengdes.2022.113159
12. G. Suárez López, "The performance of EU-DEMO under different wave heating mixes: A look into the physics and technology of ECRH and ICRH scenarios", this conference
13. R. Ragona et al., Nuclear Fusion **62** (2) 026046, 2022, https://doi.org/10.1088/1741-4326/ac4467
14. V. Bobkov et al., Nuclear Fusion **61** (4) 046039, 2021, https://doi.org/10.1088/1741-4326/abe7d0
15. V. Maquet et al., Fus. Eng. Des. **169** 112508, 2021, https://doi.org/10.1016/j.fusengdes.2021.112508
16. M. Usoltceva et al., Plasma Phys. Control. Fusion **61** (2019) 115011, https://doi.org/10.1088/1361-6587/ab476d